# Microscopic PIV Measurements for Electro-osmotic Flows in PDMS Microchannels

Kim, M. J. *[1] and Kihm, K. D.*[2]

*1 Division of Engineering, Brown University, Providence, RI 02912, U.S.A
e-mail: Minjun_Kim@Brown.edu
*2 Department of Mechanical Engineering, Texas A&M University, College Station, TX 77843, U.S.A

***Abstract*** : Electro-osmosis is the flow produced by the action of an electric field on a fluid with a net charge, which is created by the Zeta potential and confined in the Debye layer. This basic phenomenon in the electro-kinetic transport plays an important role in the microfluidic systems being explored today because it can be applied to a variety of MEMS devices. This paper presents global and point-wise comparisons of experimental measurements of electro-osmotically driven flows in elementary microchannel configurations, which are made by photolithography using poly-di-methyl-siloxane (PDMS). To measure full field velocity distributions in PDMS microchannels, a microscopic particle image velocimetry (μ-PIV) system has been developed to track the fluorescent images of 500 nm diameter particles. Comparisons of experimental results among various micro-configurations show feasibilities of the electro-osmotic flows to use for micro-pumping and micro-fluidic flow control.

***Keywords*** : electro-osmotic flow, μ-PIV, microchannel, fluorescent micro-spheres.

# 1. Introduction

Electro-osmosis is one of the pumping mechanisms for high-performance capillary electrophoresis (HPCE). It occurs because of surface charges, known as the zeta potential (Probstein, 1993), on the non-conducting wall, such as a glass surface. This classical phenomenon of electro-osmosis reclaims its importance in devising a pumping means for microchannel flows occurring in a wide range of MEMS devices. In pressure driven microfluidic systems, the frictional forces of the mobile phase interacting at the wall of the microchannel result in radical velocity gradients throughout the microchannel. As a result, the fluid velocity is greatest in the middle of the microchannel and a substantial pressure drop along the micro-channel. On the other hand, in electro-osmotically driven systems, the electro-osmotic flow (EOF) is generated uniformly along the length of the microchannel. There is no pressure drop in the microchannel. Also, all of the solute molecules experience the same velocity component caused by electro-osmotic flow regardless of their cross-sectional position in the micro-channel because it has a plug-like flow. Therefore, the electro-osmotic flow can have various application such as a micro-pumping device, a micro-injector, DNA sequencing, etc.

The phenomenon of the appearance of a liquid flow in a capillary porous system under the influence of a constant external electric field (EEF) attracted the attention of scientists long time ago. The first qualitative views on the mechanism of electro-osmosis were advanced by Quincke in 1861. His idea was adopted by Helmholtz, who developed the electric double layer theory related the electrical and flow parameters for electro-kinetic transports in 1879. In engineering,

electro-osmosis began to be widely investigated in the late 1930s. Its application to systems of complicated composition and structure was dictated by the needs of the time. At present, there is no doubt that electro-osmosis is a phenomenon of great significance in theoretical and practical application of MEMS.

In recent years there have been numerous papers and reports on the electro-kinetic phenomenon and on μ-PIV. Meinhart *et al.* (1999) presented experimental results for PIV measurements of a microchannel flow, with emphasis on microfluidic applications. In their study, the accuracy of the PIV system was demonstrated by measuring the pressure driven flow field in a 30 μm × 300 μm × 25 mm glass rectangular microchannel. In the same year, Cummings (1999) used Ar-ion lasers to capture the flow pattern in electro-osmotically driven flow. Herr *et al.* (2000) investigated the velocity profile of flows under electro-kinetic transport with a high-resolution caged fluorescence imaging technique. These measurements showed that variations in the microchannel surface charge can cause parabolic distortions in the flow profile, indicating the presence of electro-kinetic-induced pressure gradients.

In the numerical modeling, there have also been various papers related electro-osmotic flow. Arulanandam *et al.* (2000) investigated the characteristics of electro-osmotic flow in rectangular microchannels. Also, the numerical simulation of the electro-osmotic flow revealed how the velocity field and the volumetric flow rate depend on the ionic concentration, zeta potential, channel size and the applied electrical field strength. Dutta *et al.* (2001) have developed a high-order spectral element method and verified for numerical simulation of combined electro-osmotic and pressure driven flows in complex micro-geometries.

In this paper, we start by presenting the evolution of the velocity distribution of the electro-osmotic flow in straight microchannels as well as global velocity vectors and streamlines in various micro-configurations, grooved channels that have aspect ratio of 1:1 or 1:5 respectively, and T-junction channel, under the same electric field (10 $V_{votage}$/mm). We then go on to present point-wise comparisons of the stream-wise velocity, U, and cross-stream velocity, V, in various microchannel configurations.

## 2. Experimental Setup

The use of PIV techniques is very attractive in microfluidics because it helps to understand unsteady flow phenomena. PIV techniques enable spatially resolved measurements of instantaneous flow velocity field within a very short time and allow the detection of small scale spatial structures in the flow velocity field (Meinhart *et al.*, 1999).

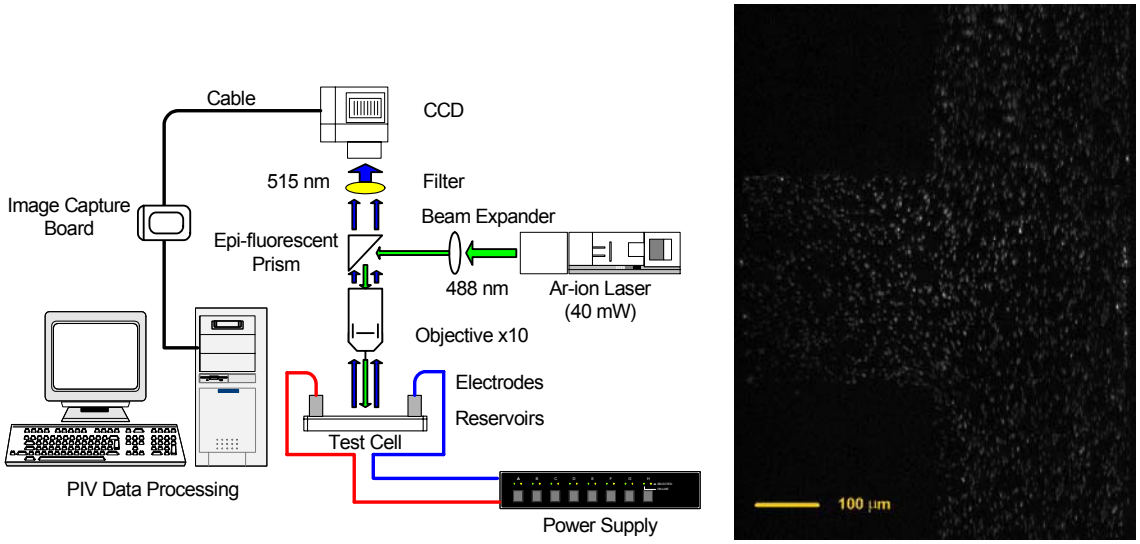


Fig. 1 Experimental setup for microscopic PIV system and PIV image in the T-junctioned microchannel

A microscopic particle image velocimetry (μ-PIV) system was developed to measure electro-osmotically driven flows in various microchannel configurations. The liquid flow in the microchannels is monitorized from the fluorescence of the seeded dye molecules. Traditional epi-illumination fluorescence microscopy is used by placing the microchannel on the microscope stage with the glass slide facing towards the objective lens (Kamholz *et al.*, 2001).

The μ-PIV utilizes flow tracing particles to map the flow in micro-geometries. In this study we use 500 nm fluorescent micro-spheres (Molecular Probes, Inc) that have an excitation peak at 490 nm and an emission peak at 515 nm. The concentration of fluorescent micro-spheres based on the interrogation volume is $7.26 \times 10^8$ particles/ml, or 0.0196 % in volume fraction. A 40 mW Ar-ion (continuous) laser beam is used to illuminate the seeding particle. Laser beam passed through a beam expander to enlarge the beam diameter, and then illuminated the test section of the microchannel, as shown in Fig. 1. The fluorescent micro-spheres are excited effectively using the 488 nm spectral line of the Ar-ion laser.

A 10× objective lens is used for magnification of the images, and the field-of-view of our experiment is 1 mm × 0.75 mm. Illuminated light passes through the objective lens and is selectively captured with a long-pass glass color filter. The fluorescence signal is recorded with an interline transfer CCD monochrome camera (Sony XC-73, Edmund Industrial Optics, NJ). The linearity of the camera response to light intensity is checked by flooding the device with different concentrations of fluorescent micro-spheres.

We have captured 20 images per second and used 640 × 480 pixels video format with the CCD monochrome camera. The PIV-measurements are evaluated with standard cross-correlation methods. Each image frame is interrogated in 32 × 32 pixels sub images with an overlap of 50 % corresponding to intervals of 16 × 16 pixels. Ensemble averaging of 80 images consecutively captured for 4 seconds is used to obtain the velocity measurements.

In the μ-PIV, the image plane should be defined by the depth-of-field of the microscope objective lens. The μ-PIV image plane thickness is much smaller than conventional PIV image planes that are defined by a thin laser sheet because microscope objectives usually have very thin depths-of-field. The formation for depth-of-field (Inoue and Spring, 1997) can be expressed as

$$\delta z = \frac{n\lambda}{NA^2} + \frac{nd_r}{M \cdot NA} \tag{1}$$

where n is the index of refraction of the immersion medium between the microfluidic device and the objectivelens (n= 1 for an air), the wavelength of illuminating light $\lambda$ = 488 nm, the numerical aperture NA = 0.25, the magnification is M = 10, and the CCD pixel size is $d_r$ = 9.0 μm. Thus, the depth-of-field of the present μ-PIV system is estimated to be $\delta z$ = 11.4 μm. Since this depth-of-field exceeds the fabricated channel depth of 7 μm, the PIV images, shown in Fig.1, effectively represent the depthwise average of the entire 7 μm deep channel flow. Either discrete particle images or a background glow arising from illuminating the entire volume of the flow filed can be minimized. For the case of the channel depths far exceeding the depth of field (Kim *et al.*, 2001), an in-depth analysis and rigorous discussions are reported for the contribution of out-of-focus particle images to the PIV correlation function (Olsen and Adrian, 2000).

The thermal Brownian diffusive motion may not be negligible when sub-micron particles are used for seeding since the particle diffusivity rapidly increases with decreasing particle diameter. The Brownian motion error, $\varepsilon_B \equiv u_B / u$ (u: characteristic velocity), is considered as having the same effect in all directions statistically. If one assumes that each particle has equal influence on the average velocity vector in the interrogation window, $\varepsilon_B$ can be reduced by averaging the number of individual particle images within the interrogation window, A, and ensemble averaging over the number of realizations, B. The Brownian motion error for PIV recording (Santiago *et al.*, 1998) is expressed as

$$\varepsilon_B = \frac{u_B}{u} \cdot \frac{1}{\sqrt{A \times B}} \tag{2}$$

For example, for a characteristic velocity of 100 μm/s from averaging of 20 image and for five

pairs of particle images within a single interrogation window, the Brownian motion error is estimated to be as little as 0.6 %.

Fabrication of the microchannels employed the rapid-prototyping "photolithography" technique using poly-di-methyl-siloxane (PDMS) (Kim *et al.*, 2002). Fluid access into the channel can be made through open-air reservoirs. The channel is terminated by reservoirs at which electrodes (Pt wire) are introduced to generate the electro-osmotic flow. The fluid used is deionized water. The measured pH and the specific conductance of the deionized water are 5.9 and 3.1 μS/cm, respectively. Because the PDMS surfaces are inherently hydrophobic, a drop of Triton X-100 non-ionic surfactant is added to the solution to lower the surface tension and to ease the process of loading the solution.

# 3. Results and Discussion

## *3.1 Straight Microchannel*

Experiments are performed with a straight microchannel that is 300 μm wide, 7 μm deep, and 22 mm long. The reservoir surfaces are initially at two equal elevations. The electrodes are placed at the inlet and outlet of the channel, and an electric field of 10 $V_{votage}$/mm is applied.

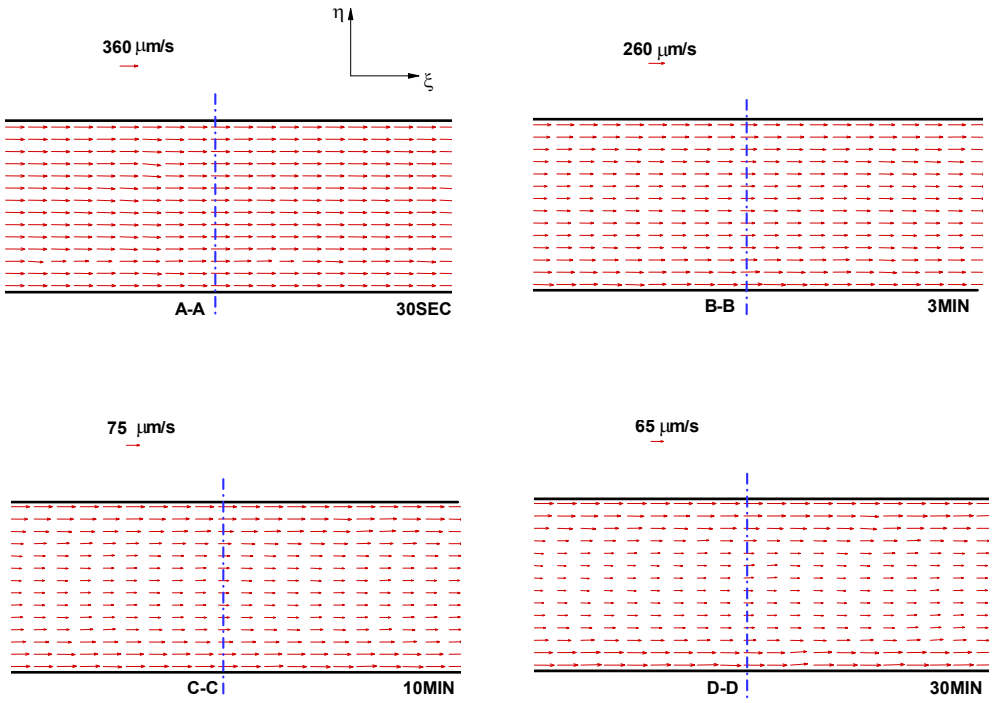


Fig. 2 Time development of the global velocity distribution for electro-osmotic flow

The measured velocity ($U_{meas}$) of a seed particle used in a microscopic PIV to quantify electro-osmotic flow is a linear superposition of the electro-osmotic ($U_{eof}$), pressure-driven ($U_{press}$), electro-phoretic ($U_{eph}$) and Brownian motion components ($U_{bm}$) of the system. In our experiments, no external pressure gradient is imposed to the flow direction and Brownian motion error is small

(0.6 %) so that $U_{press} + U_{bm} = 0$ and the total velocity field, $U_{meas} = U_{eof} + U_{eph}$. The electro-phoretic velocity ($U_{eph}$) of 500 nm fluorescent polystyrene particles, with a high density of carboxylic acids on their surface, is in general a function of the electrostatic force on the surface charge, zeta potential on their charge double layers and the viscous drag. Using the permittivity of the polystyrene particles and the electric field solution (Jones, 1995), the maximum electrophoretic force due to the applied electric field (10 $V_{votage}$/mm) can be computed to be of order $4 \times 10^{-15}$ N for the straight microchannel. A Stokes viscous drag would correspond to an electro-phoretic velocity ($U_{eph}$) of 0.49 μm/s so that electrophoresis is unlikely to influence our measurements.

Electro-osmotic flow has a plug-like velocity profile. Due to frictional drag, the electro-osmotic flow at the wall is slower than the flow through the rest of the microchannel. This reduction in flow substracts very little from the overall flat profile since the area near the wall, which is called Debye length (~100 nm), is quite small. In the fully developed electro-osmotic flow, the Reynolds number (≈ 0.05) can be calculated with an ensemble averaging velocity that has a peak speed of ~ 450 μm/s.

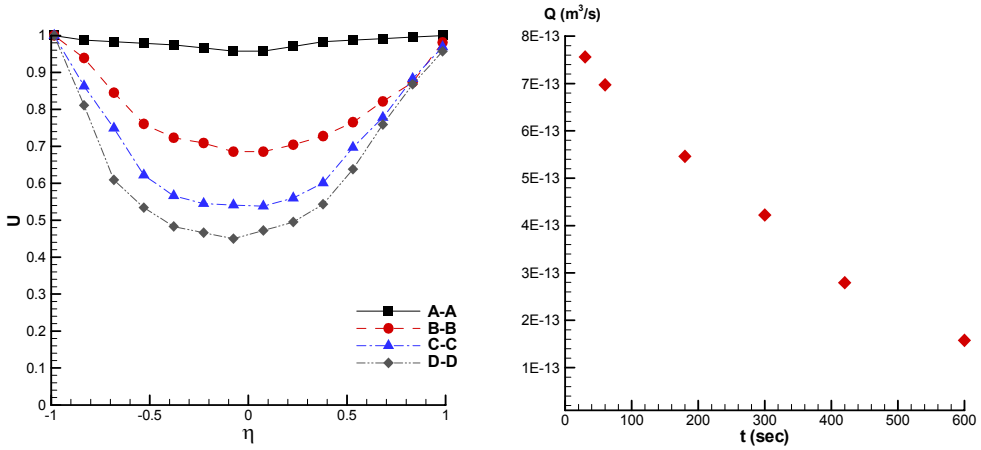


Fig. 3 Point-wise comparisons of the stream-wise (U) velocity at A-A, B-B, C-C and D-D sections (left) and volume flow-rate vs. time in the straight microchannel (right)

Fig. 2 shows time development of the global velocity distribution at indicated times after the electric field has been applied to the reservoirs. The case for $dP/d\xi = 0$, where $dP/d\xi$ is for various values of pressure gradient, corresponds to a pure plug-like flow at 30 seconds, and the cases $dP/d\xi > 0$ correspond to flow with adverse pressure gradients. By inducing adverse pressure gradients into microchannel, electro-osmotic flow can not maintain the plug-like profile. In results, average velocities of 360 μm/s, 260 μm/s, 75 μm/s, and 65 μm/s can be observed at both the inlet and exit section of the domain respectively. Fig. 3 shows that the velocity profiles after 3 minutes represent superposition of the plug-like electro-osmotic profile and the Poiseuille profile due to the adverse pressure gradient, which is resulted from the downstream reservoir height rise with flow. For this case, the inlet and the exit pressures are the same, corresponding to the microchannel that is exposed to atmospheric pressure at both ends. The entire flow is driven by the electrokinetic forces, which overcomes the drag force within the entire channel system. The pressure drops at the inlet and exit portions of the channel are due to the shear stress. The velocity after 10 minutes is very slow in comparison with fully developed electro-osmotic flow. Most PIV experiments have difficulty measuring velocity vectors very close to the wall because of hydro-dynamic interactions between the particle and the wall and background reflections from the wall overshadow particle images. By using 500 nm fluorescent particles and epi-fluorescence to remove background reflection, we have been able to make accurate velocity measurements to within about 10 μm of the wall. We can observe that volumetric flow-rate is strongly related to the averaging velocity and the adverse pressure gradient in the electro-osmotic flow. Therefore, micro-pump using electrokinetic forces must be able to raise the system pressure to be able to drive the flow. The electroosmotic pump is doing precisely this. The net pressure gradient is positive within the pump. In the case of D-D, adverse pressure gradient is present to overcome the pressure drop at the inlet and exit sections, and the net volumetric flowrate is positive, as shown in Fig. 3.

*3.2 T-junctioned Microchannels with Various Aspect Ratio*

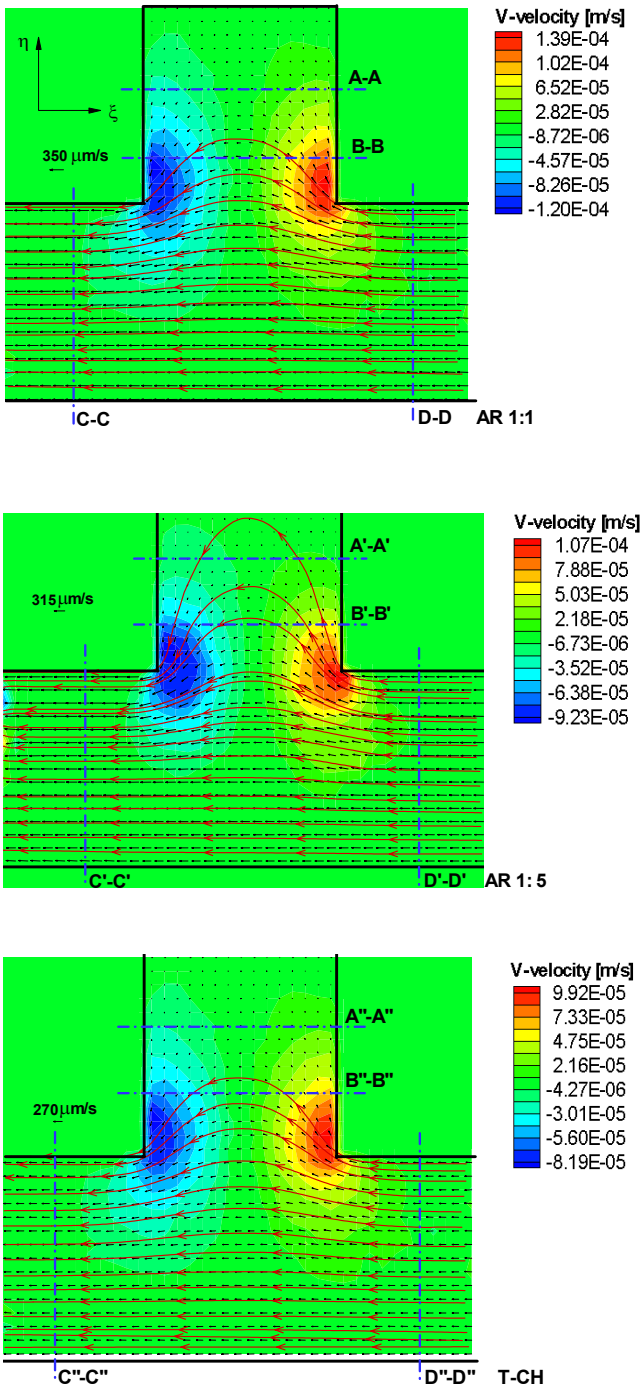


Fig. 4 The μ-PIV results in the T-junctioned microchannels (AR 1:1, AR 1:5 and AR 1:infinite) respectively. Color contour maps of velocity magnitudes are shown.

The T-junctioned-microchannels that have a cavity of 300 μm × 300 μm or 300 μm × 1500 μm create a sudden perturbation in an electro-osmotically driven straight channel flow, and locally induce a two-dimensional electric field (10 $V_{votage}$/mm). This enables us to observe the effects of a two-dimensional electric field on electro-osmotic transport. The T-junctioned microchannel has three inlet/outlet ports while two electrodes are placed so that a flow is electro-osmotically driven, while the third inlet is left open to allow a small amount of induced flow.

In Fig. 4, we present streamlines and velocity vectors of experimental results for the T-junctioned microchannels. We observe a uniform plug-like flow in the upstream (D-D, D′-D′, and D″- D″ sections) and downstream (C-C, C′-C′, and C″- C″ sections) of the cavity and the T-junction. In these regions the flow is unidirectional, while the flows near the cavity corners and the T-junction show two-dimensional flow due to the two dimensionality and corner effects. The resulting flows inside of the cavity and the T-junction are highly two-dimensional. The electric field is stronger near the first and the second corners of the cavity and the T-junction, which results in stronger electro-osmotic drive near these corners.

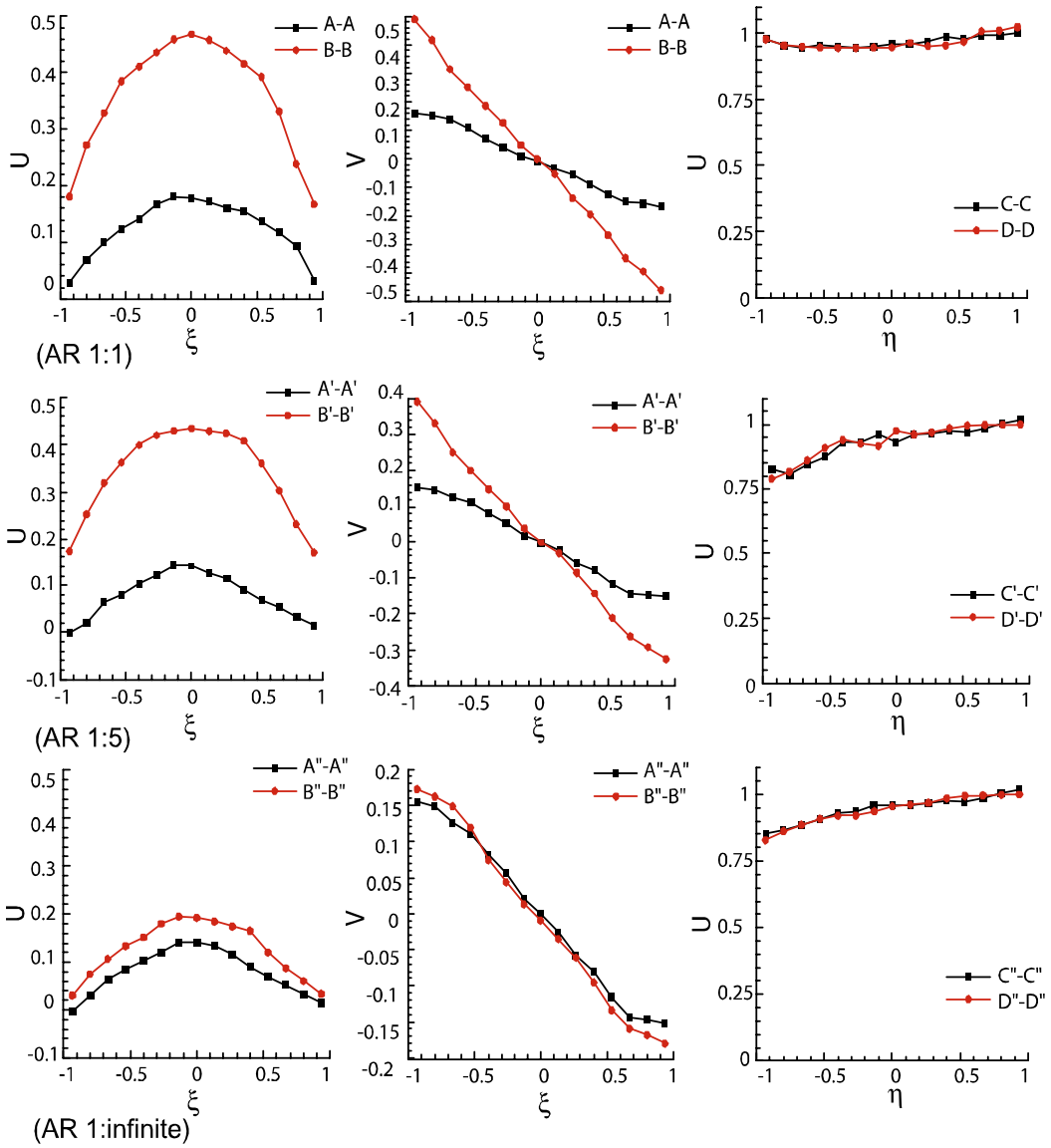


Fig. 5 Point-wise comparisons of the stream-wise velocity, U, and cross-stream velocity, V, in the T-junctioned channels (AR 1:1, AR 1:5, and AR 1:infinite) at each section

Indeed, the stream-wise velocity gradually increases along the channel wall as the flow approaches the first corner and decreases as the flow turns into the cavity and the T-junction. For the second corner, the flow accelerates as it emerges from the cavity and the T-junction and decelerates as it merges with the main stream.

Figure 5 shows quantitative comparisons of the stream-wise velocity, U, and the cross-stream velocity, V, at each section. Experimental results are normalized by a single value of the Helmholz Smoluchowski velocity, which is experimentally determined as U = 350 μm/s. The dimensionless $(\xi,\eta)$ coordinates are normalized by the channel half height h = 150 μm.

Velocity profiles at upstream and downstream show almost plug-like distribution with slight bias towards the channel wall on the cavity and the T-junction ($\eta = +1$). This is due to the increase of the electric field stress around the corners, which locally increases the electro-osmotic velocity near the corners of the T-junctioned regions. Due to the sudden expansion, the cross-stream velocity (U) becomes very prominent inside the cavity and the T-junction. Since the electric field is parallel to the surface on the cavity and the T-junction, the electric field interacts with the electric double layer, and creates large cross-stream velocity near the cavity and the T-junction walls. Since the external electric field diminishes rapidly deeper down the cavity and the T-junction, the flow field in sections A-A, A′-A′, and A″-A″ is significantly weaker than in sections B-B, B′-B′, and B″-B″.

The electro-osmotic flow would have more closely followed the electric field in the absence of adverse pressure gradient. The peak velocity is larger near the left surface ($\xi = -1$) than that at the right surface ($\xi = +1$) in Fig. 5. Since the electric field is applied asymmetrically from right to left, its stream-wise gradients are larger on the left corner than the right corner, resulting in asymmetric electro-osmotic drive in the flow field. The increasing asymmetry at section D″-D″, which is closer to the T-junction, is attributed to the increased electric field near the corner. Comparing to the flow fields in the cavities, the differences of the stream-wise velocity in the sections A″-A″ and B″-B″ of the T-junctioned channel are very small. In case of the cross-stream velocities, the similarity in the sections A″-A″ and B″-B″ is strong. These are due to the factor that the electric field can extend beyond the open reservoir in the T-junctioned channel. Therefore, when we apply an electric field to reservoirs (left to right) in the T-junctioned channel, an electro-osmotic flow into the channel of the top can be blocked effectively. In addition, we can control the electro-osmotic flow-rate by manipulating the electric field magnitude and the direction. This technique can be utilized in flow control for various microfluidic applications.

# 4. Conclusion

μ-PIV technique, which has a high accuracy and spatial resolution, is very useful in performing analysis of microfluidics such as an electro-osmotically driven flow in the microchannels. Quantitative global and point-wise comparisons are presented for time development of the velocity distribution for electro-osmotic flow in the straight microchannel using μ-PIV technique. The electro-osmotic forces can make a uniform flow, which is proportional to the local electric field. The μ-PIV results for straight microchannel can be applied to perform flow-rate control. This can be used in micro-pumping devices.

We have presented experimental results for electro-osmotically driven flows in straight channels and T-junctioned geometries. The experiments are performed for specified inlet and outlet conditions to observe pure electro-osmotic flow, in which reservoir surfaces are initially at two equal elevations. In straight microchannels, we demonstrated electrokinetic pumping and mechanisms for creating adverse pressure gradients in microfluidic systems. In T-junctioned geometries, we have shown electro-osmotic flow to demonstrate the flow behavior effectively blocked by applying the electric field to reservoirs. Hence, the T-junctioned geometries can be used as an electro-osmotically actuated microvalve with non-moving parts because the flowrate is a linear function of the electric field.


## *Acknowledgements*

The authors would like to acknowledge Dr. Ali Beskok, Dr. Prashanta Dutta and Dr. Paul Cremer for their assistance. Support from the TAMU Interdisciplinary Research Program is acknowledged and appreciated for the present work.

## *References*


Arulanandam, S., Li, D., 2000, "Liquid Transport in Rectangular Microchannels by Electroosmotic Pumping," Colloid and Surfaces A: Physicochemical and Engineering., Vol. 161, 89.

Cummings, E. B., 1999, "PIV Measurement of Electroosmotic and Pressure-driven Flow Components in Microfluidic System," Proc. of ASME MEMS., Vol. 1, 180.

Dutta, P., Beskok, A., 2001, "Analytical Solution of Combined Electroosmotic/Pressure Driven Flows in Two-dimensional Straight Channels: Finite Debye Layer Effects," Anal. Chem., Vol. 73, No. 5, 1979.

Herr, A. E., Molho, J. I., Santiago, J. G., Mungal, M. G., Kenny, T. W., Garguilo, M. G., 2000, "Electroosmotic Capillary Flow with Nonuniform Zeta Potential," Anal. Chem., Vol. 72, No. 5, 1053.

Inoue, S., Spring, K. R., 1997, "Video Microscopy," 2nd ed Plenum Press, Oxford.

Jones, T. B., 1995, "Electromechanics of Particles," Cambridge University Press, Cambridge.

Kamholz, A. E., Schilling, E. A., Yager, P., 2001, "Optical Measurement of Transverse Molecular Diffusion in a Microchannel," Biophysical Journal., Vol. 80, 1967.

Kim, M. J., Kim, H. J., Kihm, K. D., 2001, "Micro-Scale PIV for Electroosmotic Flow Measurement," In process for the 3rd Pacific Symposium on Flow Visualization and Image Processing, Paper No. F3112.

Kim, M. J., Beskok, A., Kihm, K. D., 2002, "Electroosmosis-driven Micro-channel Flows: a Comparative Study of μ-PIV Measurements and Numerical Simulations," Experiments in Fluids., Vol. 33, 170.

Meinhart, C. D., Wereley, S. T., Santiago, J. G., 2000, "PIV Measurements of a Microchannel Flow," Experiments in Fluids., Vol. 27, 414.

Olsen, M. G., Adrian, R. J., 2000, "Out-of-focus Effects on Particle Image Visibility and Correlation in Microscopic Particle Image Velocimetry," Experiments in Fluids., Vol. 26:S, 166.

Probstein, R. F., 1994, "Physicochemical Hydrodynamics," John Wiley & Sons Inc, NewYork.

Santiago, J. G., Wereley, S. T., Meinhart, C. D., Beebe, D. J., Adrian, R. J., 1998, "A Particle Image Velocimetry System Microfluidics," Experiments in Fluids., Vol. 25, 316.


## *Author Profile*

MinJun Kim: He is a Ph. D candidate in the Division of Engineering at Brown University. He received his MS in Mechanical Engineering in 2001 from Texas A&M University. He worked with Prof. Kihm in Micro-scale Fluidics & Heat Transport Laboratory of Texas A&M University as a graduate research assistant. He is affiliated at Microfluidics Laboratory and Center for Fluid Mechanics in Brown University. His research interests are bacterial flow, optical diagnostics for microfluidics and biofluidics, and micro-fabrication for MEMS devices.

Kenneth David Kihm: He is a professor of Mechanical Engineering at Texas A&M University. Prof. Kihm received his Ph.D from Stanford University in 1987. His research interests include: development and applications of laser diagnostic techniques for heat and mass transfer problems, in particular, full-field velocity and temperature mapping diagnostics in the micro-scale flows